ACS APPLIED NANO MATERIALS
Cite This: ACS Appl. Nano Mater. 2018, 1, 922−932
Article
www.acsanm.org

Folic-Acid-Functionalized Graphene Oxide Nanocarrier: Synthetic Approaches, Characterization, Drug Delivery Study, and Antitumor Screening

Marcelo de Sousa,*,† Luis Augusto Visani de Luna,*,†,‡ Leandro Carneiro Fonseca,† Selma Giorgio,‡ and Oswaldo Luiz Alves*,†

†Laboratory of Solid State Chemistry (LQES), Institute of Chemistry, University of Campinas (UNICAMP), Campinas, São Paulo CEP 13.083-861, Brazil

‡Department of Animal Biology, Institute of Biology, University of Campinas (UNICAMP), Campinas, São Paulo CEP 13.083-864, Brazil

Supporting Information

ABSTRACT: In this work, we developed and screened the potential antitumor activity of a nanocarrier based on graphene oxide (GO) and folic acid (FA) for the delivery of chemotherapy drugs. GO was synthesized by the graphite exfoliation process. FA was linked to PEG (4,7,10-trioxa-1,13-tridecanediamine) to form FA−PEG, followed by coupling to the GO surface. Camptothecin (CPT) was further adsorbed on GO for use as a drug model in the delivery study. The synthesis of the intermediate FA−PEG molecule and coupling to GO for the formation of the GO−FA nanocarrier were confirmed by basic and state-of-the-art characterization techniques, including infrared (FTIR) spectroscopy, thermogravimetric analysis (TGA), electrospray ionization (ESI) mass spectrometry, transmission electron microscopy (TEM), and magic-angle spinning carbon-13 nuclear magnetic resonance (CP/MAS ^{13}C NMR) spectroscopy. FTIR spectroscopy showed a significant reduction in the signal intensity of the carboxylic groups after the functionalization of GO with FA−PEG. TGA of GO−FA revealed that approximately 20% of the functional groups were from FA−PEG. GO−FA indicated a high CPT loading capacity (37.8%). *In vitro* studies confirmed prolonged drug release over 200 h. Acidic pH (5.0) slowed the release of CPT from the nanocarrier compared to that at physiological pH (7.4). The toxicity screening of GO−FA and GO−FA + CPT was investigated for two widely studied preclinical cell models: J774, a tumor cell with macrophage phenotype and high proliferation rate; and HepG2, a tumor cell obtained from human hepatocellular carcinoma with folate transporters. The toxicity of the GO−FA nanocarrier without drug loading was dependent on the cell type and presented no toxicity to J774 but high toxicity to HepG2. The presence of FA in the nanocarrier loaded with CPT was crucial to achieve apoptosis in both tumor cell lines. In addition, confocal microscopy revealed both the adhesion and internalization of the FITC-labeled GO−FA by the tumor cell lines.

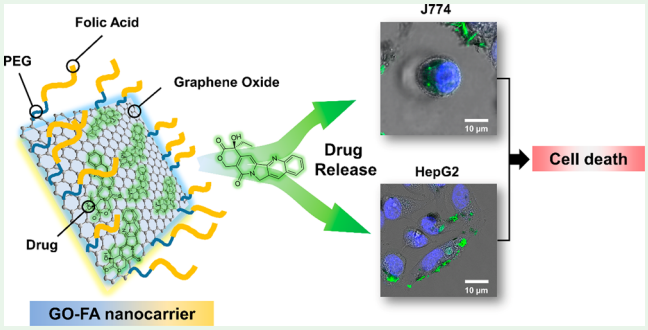

KEYWORDS: *graphene oxide, molecular vehicles, folic acid, hydrophobic drug, tumor target*

1. INTRODUCTION

Graphene oxide (GO) is a two-dimensional nanomaterial composed of single-layer sheets of sp^2 hybridized carbons, sites of sp^3 hybridized carbons, and oxygenated groups, which can be obtained from the oxidation and exfoliation of graphite.[1] This nanomaterial has attracted much interest in several fields of research, mainly due to its intrinsic physical−chemical, mechanical, and structural properties.[2] GO has been extensively studied for the delivery of drugs because it has a large hydrophobic area that allows hydrophobic drug loading by noncovalent adsorption via $\pi-\pi$ stacking and interactions with aromatic compounds.[3,4] The large GO surface and the presence of oxygenated groups allow the development of a variety of nanomaterial modification approaches, such as chemical functionalization and coating with molecules and polymers, for the creation of drug delivery systems.[5,6]

Cytotoxicity tests have shown that GO exhibits a certain degree of toxicity to cells, while the functionalization of GO with biocompatible polymers, such as polyethylene glycol, dramatically reduces the *in vitro* and *in vivo* toxicity.[7,8] In this way, the possibility of modifying the GO surface with a range of functionalizations, both covalent and noncovalent, is an important feature for successful biomedical applications. The functionalization can increase the specificity of the nanomaterial

Received: December 11, 2017
Accepted: January 30, 2018
Published: January 30, 2018

DOI: 10.1021/acsanm.7b00324
ACS Appl. Nano Mater. 2018, 1, 922−932

and guide the nanocarrier through preferential sites of action, increasing the potential for therapeutic use. Other advantages of employing a nanocarrier as a drug delivery system is the capacity to carry doses of the desired drug without considerable loss and with prolonged drug release.[9,10] In terms of functionalization, GO has a great advantage over other nanocarriers, mainly because the presence of a large amount of carboxylic groups on its surface enables the coupling of numerous molecules of interest over the amount possible with other nanocarriers such as liposomes and solid lipid nanoparticles.[11,12] In addition, a higher degree of functionalization of GO can increase the nanocarrier functionality. Furthermore, the process of GO functionalization is relatively simple compared to that for other nanomaterials because activation of the carboxylic groups present on the GO surface is easily achieved with coupling agents [e.g., *n*-(3-(dimethylamino)-propyl)-*n*-ethylcarbodiimide (EDC), *n*-hydroxysuccinimide (NHS), and thionyl chloride ($SOCl_2$)]. In addition, robust characterization techniques, such as nuclear magnetic resonance, infrared spectroscopy, and thermogravimetric analysis, among others, can follow and confirm the successful functionalization of GO. For nanocarriers such as liposomes and solid lipid nanoparticles, a high degree of functionalization is difficult to achieve because the target molecules should be coupled after the formation of the nanocarriers or added during the production process of the nanomaterials. In the first case, the nanocarriers may not present the necessary number of coupling functional groups, leading to a low degree of functionalization, and in the second case, the formulations were not stable at high concentrations of the target molecules. In addition, nanocarriers such as liposomes and solid lipid nanoparticles have limitations in terms of encapsulation, mainly due to the solubility of drugs in these matrices. GO sheets have a higher surface area than these nanocarriers, and this feature plays a crucial role in the high adsorption of molecules to the GO surface. Another advantage of GO in relation to the above-mentioned nanocarriers is the absence of high temperatures during the drug loading process, which avoids possible molecular degradation and allows the loading of thermally sensitive drugs. In this manner, some authors have observed high drug loading capacities and the sustained drug release of functionalized GO.[13,14]

Chemotherapies are based on the injection or ingestion of drugs with systemic action. However, the pharmaceutical industry has spent much effort in the development of systems able to increase the target specificity of anticancer drugs and reduce undesired effects of the systemic treatment.[15,16] In this context, the functionalization of nanocarrier surfaces has arisen as a viable alternative to improve the delivery efficacy of drugs to specific sites and reduce the dose of the administered drugs. Encouraging results were obtained with screening tests performed *in vitro* and *in vivo* using nanomaterials functionalized with folic acid (FA).[17−20] FA is a molecule with high affinity for tumor cells, inducing the internalization of nanomaterials.[21,22] This occurs because tumor cells sequestrate FA, the main donor of methyl moieties, and deregulate their gene expression by the DNA methylation mechanism. In brief, the hypermethylation and hypomethylation of DNA can lead to the silencing of essential cellular genes, triggering a disordered mitotic recombination and promoting genomic instability.[23,24] These events can be precursors of cancers and are fundamental for disease progression. In this work, we employed HepG2 hepatocellular carcinoma cells because the liver is the main reservoir of folate and folate derivatives,[25] and thus, GO−FA nanocarriers can be of interest for the treatment of liver cancer. Notwithstanding, these cells express low levels of FA receptors, but they do express reduced folate carriers (RFCs), the major transporter for folates in mammalian cells and tissues.[26,27] The mouse macrophage J774 is a tumor cell obtained from reticulum sarcoma. This cell has a macrophage-like phenotype and high capacity for proliferation. The particular interest for this cell is that J774 can actively internalize nanocarriers independently of the folate receptors and transporters. In addition, the above-mentioned cells are preclinical *in vitro* models widely reported in the literature, which permit comparison of the toxicity profile to other low-dimensional drug nanocarriers.

The development of nanocarriers functionalized with FA is a promising strategy for the effective delivery of drugs for chemotherapy. The developments of imaging systems[28] and therapeutic agents[29] are examples of using nanomaterials functionalized with FA for cancer treatment studies. In this work, we demonstrated the essential steps for the production of GO functionalized with FA for drug delivery. We employed basic and state-of-the-art characterization techniques to confirm nanocarrier functionalization. We also examined the dynamic release of drugs from the nanocarrier in two physiological conditions using sink condition and camptothecin (CPT) as a model drug. In addition, a systematic toxicity screening of the nanocarrier was performed *in vitro* for two tumor cell models, which enabled us to elucidate the role of functionalization in the tumoricidal activity.

2. EXPERIMENTAL SECTION

2.1. Materials. The following materials were used for the nanocarrier synthesis and functionalization: natural graphite powder (98%) (Synth), potassium permanganate ($KMnO_4$, 99.0%) (Synth), sulfuric acid (H_2SO_4, 95.0−98.0%) (Synth), hydrochloric acid (36.5−38.0%) (Synth), hydrogen peroxide (30.0%) (Synth), sodium hydroxide (NaOH, >99.0%, pellets) (Synth), ethanol (Synth), phosphorus pentoxide (P_2O_5) (Sigma-Aldrich), potassium persulfate ($K_2S_2O_8$, 99.0%) (Sigma-Aldrich), folic acid (FA) (Sigma-Aldrich), *n*-(3-(dimethylamino)propyl)-*n*-ethylcarbodiimide (EDC) (Sigma-Aldrich), *N*,*N*′-dicyclohexylcarbodiimide (DCC) (Sigma-Aldrich), *n*-hydroxysuccinimide (NHS) (Sigma-Aldrich), nitric acid (Synth), 4,7,10-trioxa-1,13-tridecanediamine (PEG) (Sigma-Aldrich), di-*tert*-butyldicarbonate (BoC_2O) (Sigma-Aldrich), chloroform ($CHCl_3$) (Synth), dichloromethane (CH_2Cl_2) (LSChemicals), sodium sulfate (Na_2SO_4) (Vetec), dimethyl sulfoxide (DMSO) (Synth), ether (ET_2O) (Synth), trifluoroacetic acid (Neon), *N*,*N*-dimethylformamide (DMF) (Vetec), phosphate buffer (Sigma-Aldrich), acetic acid (Synth), polysorbate 80 (Tween 80−T80) (Makeni Chemicals), polyvinylidene fluoride (PVDF) membrane filters (0.22 μm) (Millipore), dialysis tubing (12−14 kDa) (Fisherbrand), a filtration system, a condenser, a round-bottom flask, and a hot plate.

2.2. Preparation and Characterization of GO. GO was synthesized according to the modified Hummers method.[1] First, 4.4 mL of sulfuric acid was preheated to 80 °C, and 0.8 g of $K_2S_2O_8$ and 0.8 g of P_2O_5 were added to the flask, followed by the addition of natural graphite powder (1.0 g). The system was kept under constant stirring for approximately 4.5 h. Then, 170 mL of deionized water was slowly added to the flask, and the reaction was kept under stirring overnight. The next day, the system was filtrated with a PVDF membrane (0.22 μm) and washed with deionized water until reaching a neutral pH. The obtained pretreated graphite was dried at room temperature overnight. Afterward, 40 mL of sulfuric acid was added to a cooled flask (−10 °C) in a dry ice bath. The pretreated graphite was added to the flask, followed by the slow addition of 5.0 g of $KMnO_4$. The temperature was raised to 35 °C, and the reaction was kept under

DOI: 10.1021/acsanm.7b00324
ACS Appl. Nano Mater. 2018, 1, 922−932

stirring for 2 h. After this step, the temperature was decreased to −10 °C. A volume of 77 mL of deionized water was added to the flask, and the temperature was maintained below 50 °C. The reaction was continued for another 2 h at room temperature. Then, 230 mL of deionized water and 4 mL of H_2O_2 were sequentially added to the flask, and the system was allowed to settle for 2 days. The supernatant was removed, centrifuged at 3000 rpm for 30 min at room temperature, and washed with 500 mL of 10% (v/v) HCl. Subsequently, the solid was washed with deionized water by centrifugation at 15 000 rpm at 4 °C for 30 min. The resulting material was subjected to dialysis for 10 days, lyophilized, and stored. Finally, GO suspensions were obtained by dispersing the solid in deionized water with sonication in an ultrasonic bath (Cole Parmer 8891).

2.3. Synthesis and Characterization of FA−PEG. FA−PEG was synthesized according to Sahu,[30] Mohapatra,[31] Frasconi,[32] and Dhar[33] with some modifications. For this, BoC_2O (3 mmol, 0.65 g) was dissolved in 15 mL of chloroform ($CHCl_3$) cooled to 0 °C and added dropwise under stirring to a solution of 30 mmol (6.61 g) of PEG in 30 mL of anhydrous $CHCl_3$. The reaction was kept under stirring at room temperature for 24 h. Then, the solvent was removed under reduced pressure, and the obtained gummy oil was diluted in 60 mL of CH_2Cl_2. The organic phase was washed four times in 300 mL of a highly concentrated saline solution (NaCl), dried with anhydrous sodium sulfate (Na_2SO_4), and filtrated with filter paper, and the solvent was removed under reduced pressure.

In another step, 1.13 mmol of FA (0.50 g) was dissolved in 25 mL of DMSO; 20 mL of pyridine containing 1.13 mmol of DCC (0.23 g) and 2.26 mmol of NHS (0.26 g) were added, and the reaction was kept under mild stirring in the dark for 24 h. On the following day, the mixture was filtrated with a 0.22 μm PVDF membrane to eliminate reaction byproducts. FA−NHS was precipitated with a mixture of ether and ethanol and washed several times with ether. Then, 0.69 mmol of FA−NHS (0.37 g) was dissolved in 20 mL of DMSO, and 1.50 mmol of PEG−Boc (0.48 g) was added. The mixture was kept under stirring for 24 h in the dark. The next day, ether and ethanol were added to the reaction mixture, and a yellow precipitate was formed. This precipitate was washed with ether, mixed with 5 mL of trifluoroacetic acid (TFA), and stirred at room temperature for 5 h. TFA was removed under reduced pressure, and the yellow precipitate was dissolved in 15 mL of DMF. Ether and ethanol were added again to precipitate the solid, which was then washed with ether. The following steps were performed to eliminate the folic acid that did not react with PEG−Boc. The yellow precipitate was dissolved in 30 mL of ethanol; the solution was centrifuged, and the supernatant was filtrated through a 0.22 μm PVDF membrane. Afterward, ethanol was evaporated, and the resultant precipitate was washed with ether and dissolved in 25 mL of deionized water. This solution was centrifuged again and filtrated. The supernatant was lyophilized for 3 days.

The obtained compounds were characterized by electrospray ionization mass spectrometry in positive ion mode (ESI-MS) (Micromass Quattro MicroTM API from Waters), hydrogen nuclear magnetic resonance (^{1}H NMR) spectroscopy (Avance 500 mHz spectrometer), and infrared (FTIR) spectroscopy (FTLA 2000 spectrometer). This information can be found in the Supporting Information (Figures S1−S12).

2.4. Functionalization of GO with FA−PEG. A mass of 50.0 mg of GO was completely dispersed in 50 mL of DMF (1.0 mg mL^{-1}) using an ultrasound bath. EDC (0.2 g) and NHS (0.2 g) cross-linking reagents were added, and the mixture was allowed to stand for 24 h in the dark. This reaction mixture was filtrated to eliminate excess of EDC/NHS, and after this, GO-NHS was dissolved in 15 mL of DMF. For this reaction, FA−PEG (0.2 g) was added and agitated for 24 h in the dark. Then, GO−FA was washed with deionized water, using centrifugation and a vacuum pump, and dialyzed for 2 days to eliminate residual solvent. Part of the obtained material was stored in suspension, and the other part was lyophilized and stored at room temperature in a vacuum desiccator. Figure 1 illustrates the performed functionalization steps.

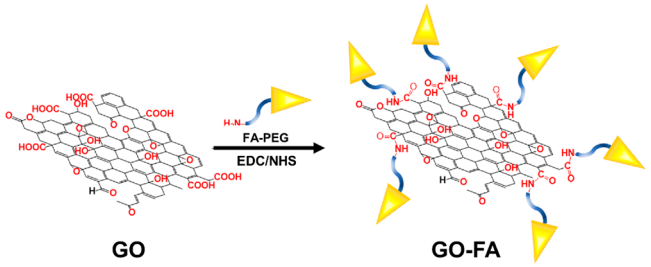

Figure 1. Scheme of GO functionalization with FA−PEG using EDC and NHS cross-linking reagents.

GO and GO−FA were characterized using the following techniques: (i) Magic-angle spinning carbon-13 nuclear magnetic resonance (CP/MAS ^{13}C NMR) spectroscopy in the solid state using a Bruker Avance II$^+$ spectrometer NMR 300 MHz. The data were analyzed with TopSpin 2.1 software. (ii) Thermogravimetric analysis (TGA) was performed with approximately 4.0 mg of dried GO and GO−FA. The thermal decomposition of the nanomaterials was analyzed under nitrogen flux at a heating rate of 10 °C min^{-1} between 30 and 1000 °C using a TA Instruments SDTQ600 model thermobalance. (iii) FTIR analyses were performed using KBr pellets in an FTLA 2000 spectrometer over the range 400−4000 cm^{-1} with a resolution of 4 cm^{-1} and 32 scans. (iv) For observation of the morphology, GO and GO−FA were dispersed in deionized water at a concentration of 10.0 μg mL^{-1}, deposited on a grid, and maintained in a desiccator for 24 h. The morphologies of GO and GO−FA were observed by TEM using a Zeiss LIBRA 120 microscope coupled to an Omega Filter spectrometer with an accelerating voltage of 80 kV.

2.5. Loading Capacity (LC%) and Loading Efficiency (LE%) of CPT in GO and GO−FA. CPT was loaded on GO and GO−FA by a simple, noncovalent, and $\pi-\pi$ interaction method. The drug was dissolved in DMSO (5.0 mg mL^{-1}), then mixed with deionized water and GO (0.5 mg mL^{-1}) and GO−FA (0.5 mg mL^{-1}) dispersions separately. The proportion of GO and GO−FA to CPT was maintained in a 1:1 (w/w) ratio. The dispersion was sonicated for 10 min and kept under agitation for 24 h protected from light. The next day, for the removal of excess of CPT from GO + CPT and GO−FA + CPT, the dispersions were filtrated (Millipore Filtration System), washed three times with methanol and deionized water in a 1:1 (v/v) ratio, and sequentially washed with deionized water, followed by the dispersion of GO + CPT and GO−FA + CPT in deionized water. During the drug loading and washing processes, the volumes of deionized water and deionized water/methanol were maintained constant to the original solution. For determination of the drug loading efficiency (LE%) and the loading capacity (LC%), 0.1 mL of a GO + CPT or GO−FA + CPT dispersion was mixed with 1.0 mL of chloroform ($CHCl_3$) and submitted to 1 min of sonication in an ultrasound bath. After sonication, 3.9 mL of methanol was added to the dispersions, and then, the mixture was submitted to an additional 10 min of sonication. The dispersions were centrifuged at 14 000 rpm for 10 min (Eppendorf Centrifuge 5424), and the presence of CPT in the supernatant was verified by UV−vis spectroscopy at 360 nm (Shimadzu model UV-1650-PC spectrometer). LE% is defined as (weight of the drug loaded on GO/weight of the drug initially added) × 100, and LC% is defined as (weight of the drug loaded on GO/weight of GO/GO−FA) × 100, as shown by eqs 1a and 1b, respectively.

$$\mathrm{LE\%} = \left(\frac{W_{\mathrm{CPT}}}{W^0_{\mathrm{CPT}}}\right) \times 100 \tag{1a}$$

$$\mathrm{LC\%} = \left(\frac{W_{\mathrm{CPT}}}{W_{\mathrm{GO}}}\right) \times 100 \tag{1b}$$

Here, W^0_{CPT}, W_{CPT}, and W_{GO} are the weight of the drug initially added, the weight of the drug adsorbed to GO, and the total weight of GO, respectively.

DOI: 10.1021/acsanm.7b00324
ACS Appl. Nano Mater. 2018, 1, 922−932

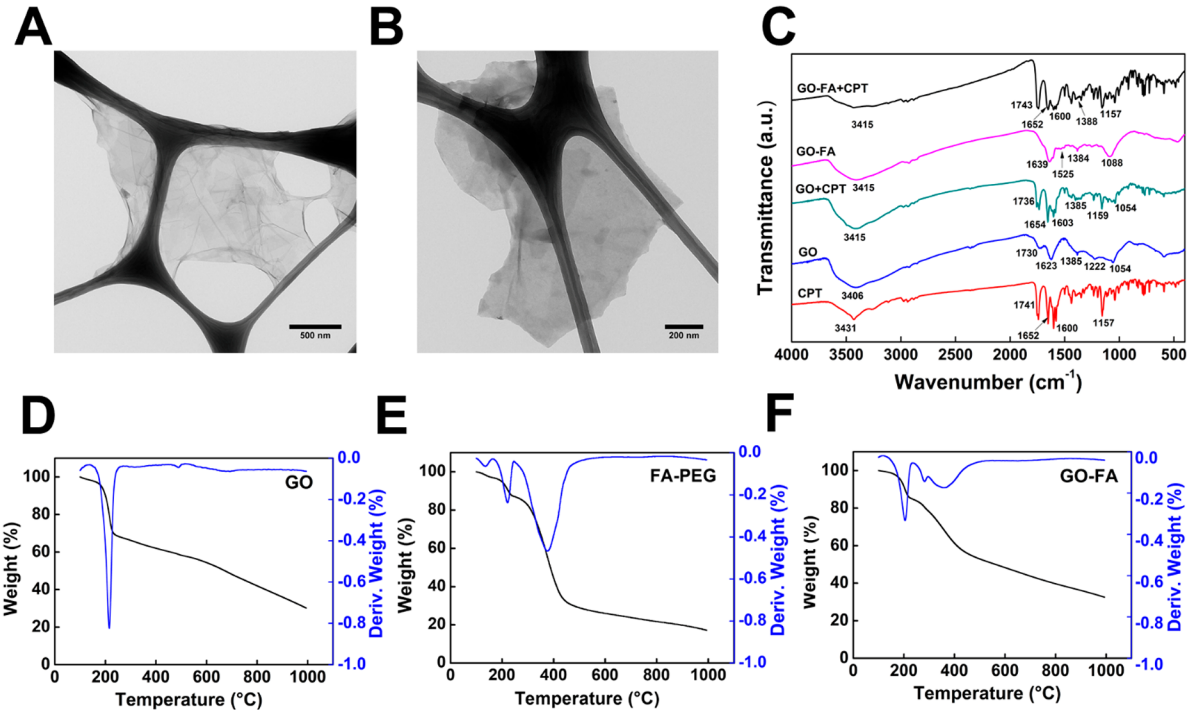

Figure 2. TEM images of GO (A) and GO−FA (B). (C) FTIR spectra of camptothecin (CPT) and nanocarriers not loaded (GO and GO−FA) and loaded with the drug (GO + CPT and GO−FA + CPT). TGA analysis of GO (D), FA−PEG bonded molecules (E), and GO−FA (F).

2.6. *In Vitro* Release Study of CPT from GO + CPT and GO−FA + CPT. *In vitro* release studies were performed according to the sink condition method. For this, 3.0 mL of preprepared GO + CPT and GO−FA + CPT dispersions (Section 2.5) were added to dialysis membranes (Spectra/Por; MWCO: 3.5 kDa). The loaded membranes were immersed in 100 mL of PBS buffer (pH 7.4) or acetate buffer (pH 5.0) containing 1% (v/v) Tween 80, a nonionic surfactant, to maintain the sink condition. The loaded membranes were maintained at 37 °C, and samples were taken at predetermined intervals. After each sample was taken, the same volume of the corresponding buffer was added to the system to maintain a constant volume. The amount of released drug present in the dispersion medium was determined by UV−vis spectroscopy, as described before. The percentage of released drug was calculated in relation to the total of CPT obtained in the previous item. The analyses were performed in triplicate.

2.7. Toxicity Assessment for the Tumor Cell Lines. The tumor cell lines used in this study were obtained from BCRJ cell bank (Banco de Células do Rio de Janeiro, Rio de Janeiro, Brazil). Prior to the toxicity tests, tumor macrophages J774 were cultivated in cell culture bottles with RPMI 1640 medium containing 10% of fetal bovine serum (FBS), and HepG2 cells were cultivated in DMEM with high glucose containing 10% of FBS. The cells were cultivated under 5% CO_2, 5% O_2, and balanced N_2 with 80% humidity at 37 °C. The general procedures adopted for the toxicity assessment of GO, GO−FA, and the CPT-loaded nanocarriers are described below. Approximately 1×10^5 cells were plated in 24-well sterile microplates and allowed to adhere for 24 h. The next day, the cell culture medium was replaced by a new medium containing the dispersed nanomaterials, both with and without CPT loading, and then, the microplates were incubated in a cell culture chamber for 24 h. The following concentrations were tested: 13.6 μg ml^{-1} GO, 18.4 μg ml^{-1} GO−FA, and 20 μM CPT. Cells without exposure to the nanocarriers were considered negative controls, and CPT (20 μM) alone was used as a positive control. After 24 h of exposure, cell death was analyzed with a commercial annexin V/propidium iodide (PI) kit available for flow cytometry (BD Biosciences). In this assay, the cell supernatant was removed from each well and separated from the cells. The adherent cells were detached from the microplate with a nonenzymatic cell dissociation buffer (Sigma). Afterward, both cells and supernatant were mixed and centrifuged for 10 min at 1500 rpm at 10 °C. After that, the cell pellet was suspended in a staining buffer (BD Biosciences), incubated for 15 min with annexin V−FITC antibodies and PI (propidium iodide), and protected from light exposure. Apoptosis and necrosis of the cells were analyzed by flow cytometry (FACS Canto II, BD Biosciences). The obtained data were analyzed by FlowJo V10 and FACSDiva (BD Biosciences) software. The percentages of early apoptosis and late apoptosis/necrosis were plotted using Origin 8.5 software (OriginLab). The GO−FA stability in cell culture media was investigated as well. For this, GO−FA (18.4 μg mL^{-1}) was dispersed with ultrasound bath in deionized water, RPMI 1640 supplemented with fetal bovine serum (FBS), and DMEM rich in glucose supplemented with FBS. Digital images of the dispersions were acquired during 7 days (Figure S13).

2.8. Investigation of the Interaction of FITC-Labeled GO−FA with the Tumor Cell Lines. For an investigation of the interaction between GO−FA and the tumor cells, the nanocarrier was functionalized with fluorescein 5(6)-isothiocyanate (FITC) (>90% Sigma), a fluorescent dye with an excitation at 490 nm and emission at 525 nm. For this, ∼1.5 mg of FITC was dissolved in 1.0 mL of deionized water, which was then slowly added to 10.0 mL of a GO−FA dispersion (0.5 mg mL^{-1}) and kept under stirring for 24 h protected from light. The following day, the dispersion was washed several times with deionized water, using centrifugation (14 000 rpm, 30 min) and a filtration system (Millipore system and 0.22 μm PVDF membrane), until the nonadsorbed FITC was eliminated. To analyze the GO−FA/cell interaction, the cells were cultured in wells containing glass slides for confocal microscopy, RPMI medium, and 10% FBS, and with the dispersed GO−FA + FITC at a nontoxic concentration. The cells were incubated under 5% CO_2, 5% O_2, and balanced N_2 at 80% of humidity and 37 °C. After exposure, the RPMI medium was removed, and the cells were washed with phosphate saline buffer (PBS). Both cells were incubated with Hoechst 33342 (BD Pharmigen) for DNA staining and appropriate cell localization. After 30 min of incubation, the cells were visualized by confocal microscopy (TCS, SP5 II, Leica).

DOI: 10.1021/acsanm.7b00324
ACS Appl. Nano Mater. 2018, 1, 922−932

3. RESULTS AND DISCUSSION

3.1. Characterization of GO and GO−FA. The TEM images in Figure 2A,B show the morphology of GO before and after functionalization with FA−PEG, respectively. The presence of transparent sheets of GO (Figure 2A) indicates that the employed oxidation method was efficient to exfoliate and oxidize the graphite. In Figure 2B, dark sheets of GO functionalized with FA−PEG are observed. Despite the different composition of GO−FA, no morphological alterations were observed, revealing that the functionalization method used is an efficient alternative to link FA to structures such as GO.

The FTIR spectra for GO and GO−FA are shown in Figure 2C. For GO, the wide and intense band observed at 3406 cm^{-1} was assigned to νOH, and the bands at 1730, 1623, 1222, and 1054 cm^{-1} were assigned to νC═O, νC═C, νCO, and νCOC, respectively.[34−36] The reduction of the carboxylic band at 1730 cm^{-1} in the GO−FA spectrum provides additional confirmation of FA−PEG functionalization. Instead, we observed an intense band at 1639 cm^{-1}, resulting from the combination of the formation of an amide bond between GO and FA−PEG and νC═C. Moreover, FA−PEG presents amide groups, which contribute to the increase in the intensity of this signal. Other bands attributed to GO−FA are observed at 3415 cm^{-1} (νOH), 1384 cm^{-1} (δOH/δCH), and 1088 cm^{-1} (νCN), along with several bands between 1088 and 1639 cm^{-1}.

TGA analysis was employed to estimate the degree of functionalization of GO with FA−PEG. This analysis was not performed in synthetic air because GO decomposition occurs at the same temperature as FA−PEG decomposition. However, under nitrogen atmosphere, it was possible to obtain an estimate of the degree of functionalization, since FA−PEG decomposition occurs at a different temperature than GO decomposition under these conditions. Figure 2D−F presents the TGA and DTGA analysis of GO and GO−FA.

Figure 2D highlights a thermal event between 148 and 261 °C, which corresponds to the thermal decomposition of the oxygenated functional groups of GO. Figure 2E presents a thermal event between 232 and 505 °C. The same thermal event was observed for FA−PEG and corresponds to the thermal decomposition of the functional groups of this molecule. The observed mass loss was 12.0% and 32.3% for GO (Figure 2D) and GO−FA (Figure 2F), respectively. The difference between these mass losses is approximately 20.3%, which corresponds to the functional groups of FA−PEG coupled to GO. This value can be considered an estimative of the degree of functionalization of GO with FA−PEG, since the carbon mass of FA−PEG does not decompose under nitrogen atmosphere.

The characterization results showed that the functionalization methodology was very efficient in coupling FA−PEG to GO. On the basis of the literature results, it was possible to perform a detailed study of the chemical nature of the nanomaterials and molecules obtained in this work. CP/MAS ^{13}C NMR spectroscopy was employed to provide insight into the chemical and structural changes of GO after functionalization with FA−PEG. Figure 3A,B shows the CP/MAS ^{13}C NMR spectra of GO and GO−FA, respectively.

The GO spectrum (Figure 3A) matches the reported spectra in the literature.[37−41] Chemical shifts were observed at 59.33, 70.40, 104.39, 124.94, 161.86, and 191.11 ppm, attributed to epoxy (C—O—C), hydroxyl (C—OH), lactol (O—C—O), sp^2 carbon, carboxylic (O—C═O), and ketone (C═O) groups, respectively. The large amount of these oxygenated groups and carboxylic groups is essential in the functionalization process. The GO−FA spectrum indicates several chemical shifts related to the GO and FA−PEG molecules used in the functionalization process (Figure 3B). An excellent signal-to-noise ratio was observed, indicating the high degree of functionalization with FA−PEG. The chemical shifts of the epoxy (C—O—C), hydroxyl (C—OH), sp^2 carbon, carboxylic (O—C—O), and ketone (C—O) groups were observed at 61.59, 70.05, 129.23, 163.28, and 109.62 ppm, respectively. An intense chemical shift was not observed for lactol, indicating that the chemical structure of GO changes after functionalization. The presence of other chemical shifts is due to FA−PEG coupling to GO. The chemical shifts observed in the CP/MAS ^{13}C NMR spectra can be divided into four characteristic chemical shift regions, assigned to alkyl C (0−45 ppm), O/N alkyl C (45−110 ppm), aromatic C (110−160 ppm), and carboxyl/carbonyl C (160−220 ppm).[42−44] In the GO−FA spectrum, the chemical shift at 29.91 ppm was attributed to the CH_2 alkyl group of FA and CH_2 alkyl groups of PEG, and the chemical shift at 37.26 ppm was attributed to the other CH_2 alkyl group of FA (Figure 3B). This attribution is based in the FA spectrum given in the literature[45−47] and the FA and FA−PEG CP/MAS ^{13}C NMR spectra (Figure S9). As shown in the Supporting Information, the chemical shift in the FA−PEG spectrum at 29.60 ppm probably corresponds to the chemical shift at 29.91 ppm in the GO−FA spectrum, and the chemical shift in the FA−PEG spectrum at 36.84 ppm possibly corresponds to the chemical shift at 37.26 ppm in the GO−FA spectrum. In Figure 3B, the intense peak at 70.05 ppm is in the region of N/O alkyl chemical shifts and originated from the CH_2—O— and CH_2—NH_2/CH_2—NH structures of PEG.[42,43,45] The chemical shifts corresponding to the C-substituted aromatic carbons occur in the region 110−140 ppm, while those for O- and N-substituted aromatic carbons occur between 140 and 160 ppm.[42−49] Therefore, we can conclude that the chemical shifts at 151.17 and 155.12 ppm are due to the N-substituted aromatic carbons from the FA moieties.[50,51] The chemical shift at 172.80 ppm was attributed to both the carbon in the amide group of the FA structure and the bond formed between FA−PEG and GO.[48−52] These chemical shifts demonstrate that the employed functionalization method was efficient to bond FA−PEG to GO.

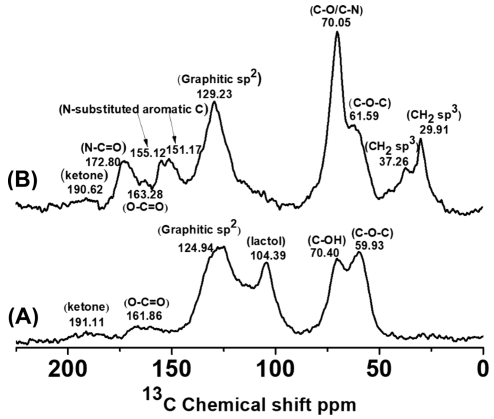

Figure 3. CP/MAS ^{13}C NMR spectra of GO (A) and GO−FA (B). The ^{13}C chemical shifts in these spectra show the chemical bonds and high degree of functionalization of GO with FA−PEG.

DOI: 10.1021/acsanm.7b00324
ACS Appl. Nano Mater. 2018, 1, 922−932

3.2. Loading Capacity (LC%), Loading Efficiency (LE %), and Drug Release Study of GO + CPT and GO−FA + CPT. Camptothecin (CPT) is a well-known hydrophobic antitumor drug and can be used for testing nanocarriers in delivery studies. This molecule was selected as a model drug to evaluate the loading capacity (LC%) and loading efficiency (LE %) of the GO−FA nanocarrier. CPT is absorbed on the surface of the GO sheets through hydrophobic interactions and $\pi-\pi$ stacking between the aromatic rings of both systems. The steps for loading the nanocarrier with CPT included dissolving the drug in DMSO, followed by addition to GO or GO−FA dispersions, and then keeping this mixture under stirring for 24 h. Excess CPT that was not absorbed to the aromatic plane of GO and GO−FA was removed by washing with a deionized water/methanol mixture, followed by several washings with water. The loading was confirmed by the presence of characteristic absorption bands in the FTIR spectrum (Figure 2C). CPT (99% purity) presents several intense characteristic absorption peaks in the FTIR spectrum. The main characteristic bands were observed at 3431, 1741, 1652, 1600, and 1157 cm^{-1}. These bands correspond to νOH, carbonyl stretching of the cyclic ester (lactone), νC═O (pyridone), νC═C, and νC—C(═O)—O, respectively.[53,54] These bands were also observed in the functionalized nanomaterials, which confirms the adsorption of CPT on the GO−CPT and GO−FA + CPT nanocarriers (Figure 2C).

For the quantitative analysis and estimation of CPT loading on the GO and GO−FA nanocarriers, the loaded nanomaterials were dissolved in methanol and sequentially submitted to sonication and centrifugation. After these steps, the supernatant was analyzed by UV−vis spectroscopy at 360 nm. In this procedure, the adsorbed drug leached from the nanomaterial surface permitted comparison with the amount of drug initially added (LE%) per weight of GO (LC%). Table 1 shows the LC % and LE% of GO + CPT and GO−FA + CPT.

Table 1. Percentage of CPT Loading to the Nanocarriers (n = 3)

	LC (%)	LE (%)
GO + CPT	52.3% (±1.0%)	53.2% (±1.0%)
GO−FA + CPT	37.8% (±0.5%)	32.6% (±0.4%)

The values of LC% and LE% were similar because of the ratio (w/w) of CPT to GO or GO−FA was 1:1. GO + CPT exhibited a higher LC% and LE% than GO−FA + CPT. These results clearly indicate that CPT was successfully loaded on GO and GO−FA.

The functionalization of GO with FA−PEG reduced the interaction between the GO sheets and CPT. The LC% and LE % of GO−FA + CPT were lower than those of GO + CPT. The presence of PEG chains increased the GO surface hydrophilicity, reducing the distance between the aromatic rings of GO and CPT. This phenomenon may diminish the available number of aromatic sites at which the drug can interact, since the sites are partially covered by FA−PEG molecules. Furthermore, the degree of loading of these nanomaterials was higher than that of other nanocarriers, such as liposomes[55,56] and solid lipid nanoparticles,[57,58] which is a great advantage over conventional nanocarriers because a higher concentration of drugs can be delivered. For liposomes and solid lipid nanoparticles, the drug should be dissolved or added inside a matrix during the drug loading process. Because of the limited solubility of hydrophobic drugs in these matrices, the loading capacities are generally smaller than those observed for GO and GO−FA. In addition, a considerable amount of drug is lost during the synthesis of liposomes and solid lipid nanoparticles.

The interaction of CPT with the surface of GO and GO−FA can be affected by changes in the pH. Therefore, release studies were performed at pH 7.4 and 5.0, which correspond to physiological pH and the pH found in lysosomes (acidic organelles of cells), respectively. Water dispersions of nanomaterials, such as GO and GO−FA, are a favorable environment for loading hydrophobic drugs that contain aromatic rings because of the poor solubility of the drug in the dispersion media and the strong $\pi-\pi$ interactions between the drug molecules and GO. Then, use of nonionic surfactants for hydrophobic drug release assay is largely employed in pharmaceutical studies because of dramatically increasing the solubility of drugs in the media and allowing the molecules to be released from the nanocarrier.[59] In this way, a nonionic surfactant was added to the receptor medium (1% Tween 80) in such a way that CPT was very soluble (sink condition) and could be released from the GO and GO−FA surface. This method was employed to estimate the release profiles of the CPT-loaded GO and GO−FA *in vitro*. This was an indirect measure of the interaction strength between the drug and the nanocarriers (Figure 4).

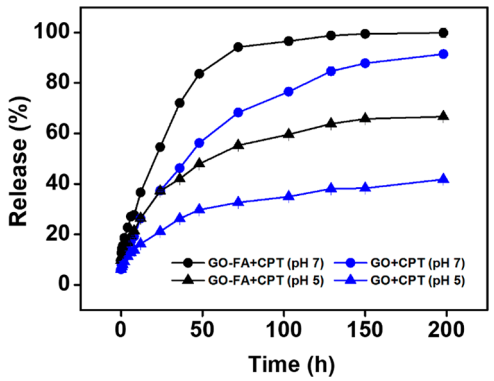

Figure 4. *In vitro* release kinetics of CPT-loaded GO and GO−FA at pH 7.4 and 5.0 (n = 3).

CPT release from the nanocarriers occurred slowly and was time-dependent in all experiments. However, the release was faster at pH 7.4 than at pH 5.0, which demonstrates the pH-dependent drug release. A possible explanation for this behavior is that, at pH 7.4, the CPT lactone ring is readily hydrolyzed and converted to the open carboxylate form.[60,61] This form is more soluble in water than the lactone ring form, which facilitates the release of CPT to the medium. Furthermore, the lactone ring can increase the interaction between the drug and the aromatic rings of GO, which retards the CPT release from the nanocarrier. Yang et al. showed that CPT in the lactone ring form plays a fundamental role in the antitumor activity and found that CPT in the carboxylate form is inactive against various tumor cells.[62] However, in acidic environments, the carboxylate form is again converted to the lactone form, and CPT becomes active against tumor cells.[60,63] According to the observed release kinetics, CPT interacts more strongly with GO, as GO + CPT showed a slower release profile than GO−FA + CPT under the same pH conditions. This observation

DOI: 10.1021/acsanm.7b00324
ACS Appl. Nano Mater. 2018, 1, 922−932

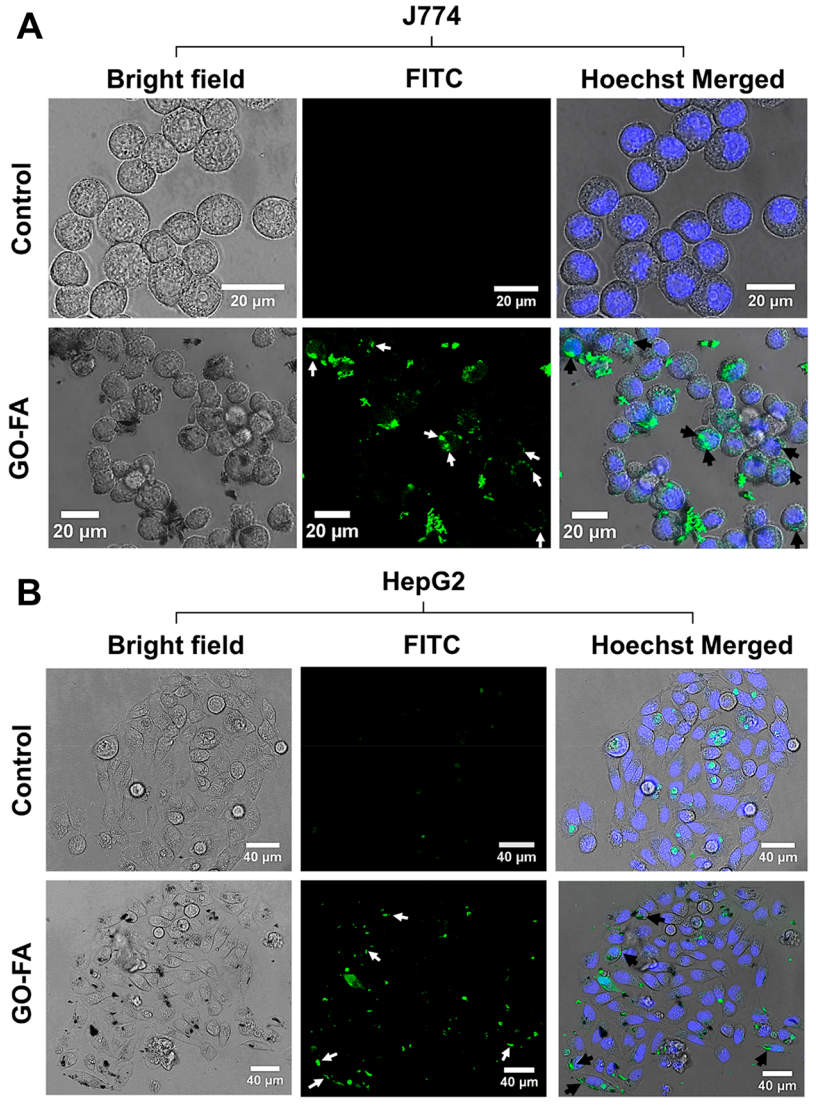

Figure 5. Confocal images of J774 (A) and HepG2 (B) cells exposed to FITC-labeled GO−FA nanocarriers without drug loading. The white arrows indicate the J774 cells with internalized FITC-labeled GO−FA. The black arrows indicate the FITC-labeled GO−FA nanocarriers adhered to the HepG2 surface.

agrees with the results and discussions of the LC%, in which we found the highest loading capacity for GO + CPT. For GO−FA + CPT, the CPT release reached 83% after 48 h, and after 100 h, it reached a plateau at which approximately 100% of the drug was released to the medium. At pH 5.0, the same nanomaterial released 48% of the drug after 48 h, which is approximately 1.73-fold slower in relation to the same time-point observation at pH 7.4. After 100 h, 60% of CPT was released to the medium, and at this time point, the drug release was reduced. For GO + CPT, at pH 7.4, the drug release reached 56% after 48 h and reached a plateau after 200 h, at which 90% of the drug was released to the medium. At pH 5.0, this nanocarrier presented the slowest release. After 48 h, 29% of the CPT was released, while at 200 h, only 41% was released from the nanocarrier. These results indicate that CPT has a stronger interaction with the GO surface than the GO−FA surface. In summary, the interaction of CPT and release from the nanocarriers were modulated by the pH changes, due to the equilibrium reaction between carboxylic groups and lactone rings of the drug as previously described.

These results show a different release profile than those reported in the literature. Kavitha et al. observed a faster CPT release mechanism at acidic pH (acetate buffer, pH 5.0−5.5) than at neutral pH (PBS buffer, pH 7.4).[64,65] This effect was attributed to the increased hydrophilicity and higher solubility of CPT at lower pH. The authors suggested that, at low pH, the nitrogen in CPT is protonated, and the hydrophobic interactions between the drug and the functionalized GO are reduced, which increases the CPT solubility in the dispersion medium. However, these authors did not mention the use of surfactants in the receptor medium (sink condition); in addition, GO was functionalized with polymers, which may be one of the reasons for the different CPT release profile.

3.3. *In Vitro* Toxicity of GO−FA Nanocarriers and the Model Drug for the Tumor Cell Lines. The interaction of GO−FA with the tumor cell lines was first verified by confocal microscopy. For this, the nanocarrier labeled with FITC was incubated with the following cell lineages: a mouse macrophage tumor cell line (J774) and a human hepatocellular carcinoma cell line (HepG2). The images depicted in Figure 5A highlight

DOI: 10.1021/acsanm.7b00324
ACS Appl. Nano Mater. 2018, 1, 922−932

the interaction of nanocarriers with J774 cells, while those in Figure 5B highlight the interaction with HepG2 cells.

Particularly for GO, its planar shape and large available surface area contribute to its adhesion on cell membranes.[66] This intimate interaction can maximize drug delivery and enhance the antitumor activity. HepG2 cells are highly adherent to substrates and present a well-spread morphology, which facilitates the interaction between GO−FA and their surface (black arrows). Considering the internalization of GO−FA by J774, Luna et al. observed that this cell presents a high uptake capacity of GO nanomaterials.[67] In Figure 5A, the internalized labeled nanocarriers can be observed (white arrows).

CPT-based drugs, such as irinotecan hydrochloride (Camptosar), are approved by the FDA (U.S. Food and Drug Administration) and can be found on the market. According to the National Institute of Health (NIH), Camptosar has been used for the treatment of colorectal and metastatic cancers. The basic toxic mechanism of CPT to cells is the inhibition of an enzyme essential for DNA replication, called topoisomerase I (topo I). This drug stabilizes the cleavable complex between topoisomerase I and DNA, resulting in DNA breaks, inhibition of DNA replication, and cell death by apoptosis.[68]

Apoptosis, well-known as "programmed cell death", is a process characterized by a metabolic cascade of caspase enzymes and transcription factors that induce DNA fragmentation, collapse of the nucleus envelope, and cytoskeleton disassembly. Cells with triggered apoptosis form large vesicles (apoptotic bodies) and present in their surface a particular phospholipid called phosphatidylserine that signalizes and alerts neighboring cells. These are characteristics of early apoptotic events. Otherwise, late apoptosis is an irreversible condition characterized by complete cytoskeleton dismantling, cell permeation, and fragmentation. The advantages of apoptosis induction in tumor cells rely on the capacity to avoid an inflammatory response occasioned by other cell death mechanisms.[69] Necrosis, however, can be characterized by acute damage to cell membrane and consequent lysis. Late apoptosis and necrosis were not distinguished by the employed assay method, and they were treated as cell death. Considering this, we explored the antitumor effects of CPT loaded in the GO−FA nanocarriers and their counterparts. The tested concentrations were 7.0 μg mL^{-1} (20 μM) of CPT, 13.6 μg mL^{-1} of GO, and 18.4 μg mL^{-1} of GO−FA nanocarriers. For the control experiments, CPT and the nanocarriers without drug loading were tested at the same concentrations described above. Figure 6A−D highlights the early and late apoptosis/necrosis events triggered by the nanocarriers with and without CPT loading. Similar capital letters indicate that there were no significant differences in the early apoptosis events, and similar lower-case letters indicate that no significant differences were observed in the late apoptosis/necrosis events.

Neither the GO nor the GO−FA nanocarriers induced significant early or late apoptosis/necrosis in the J774 cells (Figure 6A). CPT alone induced 39% of early apoptosis and 2.5% of late apoptosis/necrosis after 24 h of exposure (Figure 6B). GO + CPT induced approximately 40.9% of early apoptosis and 16.1% of late apoptosis/necrosis. In contrast, the most pronounced effects were observed for the cells exposed to GO−FA + CPT, with 57.2% of early apoptosis and 23.4% of late apoptosis/necrosis after 24 h (Figure 6B). The observed differences between GO + CPT and GO−FA + CPT may be due to the fact that J774 cells can actively internalize high amounts of GO nanomaterials, but for GO−FA in particular, the receptor-mediated internalization triggered by FA probably increased nanocarrier endocytosis.

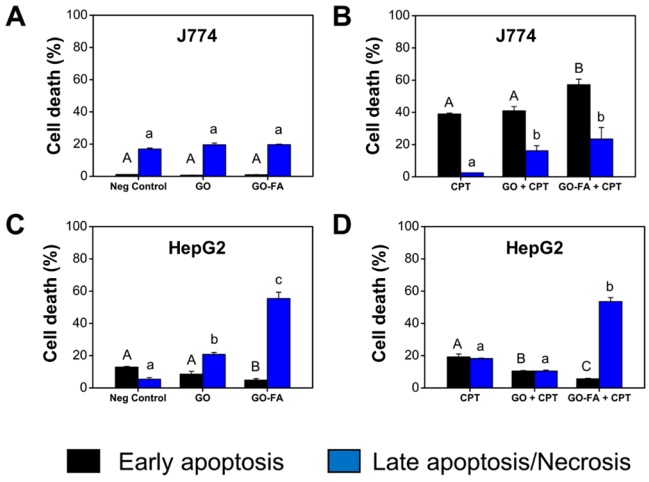

Figure 6. Percentages of early and late apoptosis/necrosis of J774 cells not exposed and exposed to the GO and GO−FA nanocarriers (A) and exposed to CPT or the nanocarriers loaded with CPT (B). Early and late apoptosis/necrosis percentages of HepG2 cells not exposed and exposed to the GO and GO−FA nanocarriers (C) and exposed to CPT or the nanocarriers loaded with CPT (D). The capital letters compare early apoptosis, and the lower case letters compare late apoptosis/necrosis ($P < 0.05$).

GO did not induce high levels of early apoptosis in the HepG2 cells (Figure 6C). However, GO−FA induced significant late apoptosis/necrosis to those cells (55.4%) (Figure 6C). The drug alone induced 19.2% and 18.2% of early and late apoptosis/necrosis, respectively. Interestingly, the GO + CPT effect was reduced by approximately half compared to CPT alone (Figure 6D). GO−FA + CPT induced low levels of early apoptosis (5.6%) but considerable levels of late apoptosis/necrosis (53.5%), as observed in Figure 6D. Again, the presence of FA on the GO surface demonstrated its importance in the toxicity to the tumor cell lines. As previously mentioned, the ability of HepG2 cells to spread increased the available cell surface for GO−FA attachment (as observed in the confocal images in Figure 5B).

Comparison between the two widely used preclinical cell models permitted us to distinguish the cell death induced by the nanocarriers. In addition, the designed study permitted the elucidation of the role of FA functionalization on the GO surface in the tumoricidal activity of the nanocarriers. Ranji-Burachalo et al. observed that FA functionalization was essential for the antitumor activity of inorganic metallic nanoparticles.[70] Furthermore, a similar nanocarrier based on folic acid conjugation to GO developed by Tian et al. showed efficient CPT delivery and apoptosis induction on HeLa tumor cells.[20]

The GO−FA stabilities in RPMI 1640 and DMEM high-glucose cell media were investigated during 7 days in the presence of fetal bovine serum (FBS). The same concentration of the *in vitro* toxicity tests was used (18.4 μg mL^{-1}). The images of each dispersion can be found in the Supporting Information (Figure S13). The nanocarrier was considered partially stable in both cell culture media. During the functionalization of GO with FA−PEG, PEG alone, other molecules and/or nanoparticles, GO can be reduced.[40] The "loss of oxygenate groups" and "reconstitution of aromatic rings" can decrease the GO stability in aqueous media. In this work, the intensity of the chemical shift of 129 ppm,

DOI: 10.1021/acsanm.7b00324
ACS Appl. Nano Mater. 2018, 1, 922−932

represented by the graphitic sp^2 domain, increased (Figure 3B). In addition, after functionalization of GO with FA−PEG, the FTIR spectroscopy showed a decrease in the intensity of the signal of carboxylic groups (Figure 2C). Probably, this reduction of GO after functionalization with FA−PEG can decrease the nanocarrier stability in the cell media.

4. CONCLUSION

We demonstrated that graphene oxide functionalized with folic acid (GO−FA) can be an alternative nanocarrier to liposomes and solid lipid nanocarriers for the delivery of hydrophobic antitumoral drugs, with perspectives for the future cancer treatment. The employed characterization techniques demonstrated that GO was efficiently functionalized with FA−PEG. CP/MAS ^{13}C NMR spectroscopy presented intense and characteristic signals of FA−PEG coupled to GO−FA. The thermal decomposition obtained by TGA analysis indicated that GO was highly functionalized with FA−PEG. The morphology of the GO sheets was not altered after functionalization with FA−PEG, as indicated by TEM. Both GO and GO−FA showed a high loading capacity and loading efficiency. However, GO−FA promoted prolonged and sustained camptothecin release. The release studies also demonstrated that drug release from the nanocarrier was slower at acidic pH (endosomal pH) than at physiological pH. The preclinical screening tests indicated that GO−FA was efficiently internalized by J774 cells and strongly adhered to the surface of HepG2 cells. The GO−FA + CPT nanocarrier promoted tumor cell death by apoptosis, but early and late apoptosis/necrosis were dependent on the cell type. In addition, FA was essential for promoting apoptosis in both cells. Additional *in vitro* and *in vivo* experiments will be performed to understand the nanocarrier selectivity and action for other preclinical tumor models. We believe this work will improve the knowledge of research groups for the development of new low-D nanocarriers functionalized with FA and their applications for drug delivery and cancer treatment.

■ ASSOCIATED CONTENT

Supporting Information

The Supporting Information is available free of charge on the ACS Publications website at DOI: 10.1021/acsanm.7b00324.

Reaction of the folic acid (FA) with PEG forming FA−PEG, characterization of FA−PEG molecules, and nanomaterial stability in cell culture media (PDF)

■ AUTHOR INFORMATION

Corresponding Authors

*E-mail: marcelosousap2@yahoo.com.br.
*E-mail: luisvisani@gmail.com.
*E-mail: oalves@iqm.unicamp.br.

ORCID

Marcelo de Sousa: 0000-0002-8279-5470

Notes

The authors declare no competing financial interest.

■ ACKNOWLEDGMENTS

The authors would like to thank the National Council for Technological and Scientific Development (CNPq) and the Laboratory of Synthesis of Nanostructures and Interaction with Biosystems (NanoBioss) for the postgraduate fellowship (Proc. 381018/2017-2) and the National Institute of Science Technology and Innovation in Complex Functional Materials (INOMAT/INCT) for the financial support. We also thank the Institute of Chemistry (UNICAMP-IQ) technician staff for their help during the development of this work.

■ REFERENCES

(1) de Moraes, A. C. M.; Andrade, P. F.; Faria, A. F.; Simões, M. B.; Salomão, F. C. C. S.; Barros, E. B.; Gonçalves, M. C.; Alves, O. L. Fabrication of Transparent and Ultraviolet Shielding Composite Films Based on Graphene Oxide and Cellulose Acetate. *Carbohydr. Polym.* **2015**, *123*, 217−227.

(2) Kim, Y. J.; Kahn, Y. H.; Lee, J. H.; Hwang, Y. H.; Lee, S. M.; Choi, S. M.; Kim, W. B.; Lee, K. Impact of Synthesis Routes on the Chemical, Optical, and Electrical Properties of Graphene Oxides and Its Derivatives. *Curr. Appl. Phys.* **2015**, *15*, 1435−1444.

(3) Xu, Z.; Wang, S.; Li, Y.; Wang, M.; Shi, P.; Huang, X. Covalent Functionalization of Graphene Oxide with Biocompatible Poly(ethyleneglycol) for Delivery of Paclitaxel. *ACS Appl. Mater. Interfaces* **2014**, *6*, 17268−17276.

(4) Zhang, L.; Xia, J.; Zhao, Q.; Liu, L.; Zhang, Z. Functinal Graphene Oxide as a Nanocarrier for Controlled Loading and Targeted Delivery of Mixed Anticancer Drugs. *Small* **2010**, *6*, 537−544.

(5) Cao, L.; Zhang, F.; Wang, Q.; Wu, X. Fabrication of Chitosan/Graphene Oxide Polymer Nanofiber and Its Biocompatiility for Cartilage Tissue Engineering. *Mater. Sci. Eng., C* **2017**, *79*, 697−701.

(6) Weng, Y.; Jiang, B.; Yang, K.; Sui, Z.; Zhang, Y. Polyethyleneimine-Modified Graphene Oxide Nanocomposites for Effective Protein Functionalization. *Nanoscale* **2015**, *7*, 14284−14291.

(7) Peña-Bahamonde, J.; Miguel, V. S.; Nguyen, H. N.; Ozisik, R.; Rodrigues, D. F.; Cabanelas, J. C. Functionalization of Reduced Graphene Oxide with Polysulfone Brushes Enhance Antibacterial Properties and Reduce Human Cytotoxicity. *Carbon* **2017**, *111*, 258−268.

(8) Wu, T.; Zhang, B.; Liang, Y.; Liu, T.; Bu, J.; Lin, L.; Wu, Z.; Liu, H.; Wen, S.; Tan, S.; Cai, X. Heparin-Modified Graphene Oxide Loading Anticancer Drug and Growth Factor with Heat Stability, Long-Term Release Property and Lower Cytotoxicity. *RSC Adv.* **2015**, *5*, 84334−84342.

(9) Wei, Y.; Zhou, F.; Zhang, D.; Chen, Q.; Xing, D. A Graphene Oxide Based Smart Drug Delivery System for Tumor Mitochondria-Targeting Photodynamic Therapy. *Nanoscale* **2016**, *8*, 3530−3538.

(10) Masoudipour, E.; Kashanian, S.; Maleki, N. A Targeted Drug Delivery System Based on Dopamine Functionalized Nano Graphene Oxide. *Chem. Phys. Lett.* **2017**, *668*, 56−63.

(11) Ghiani, S.; Capozza, M.; Cabella, C.; Coppo, A.; Miragoli, L.; Brioschi, C.; Bonafè, R.; Maiocchi, A. *In Vivo* Tumor Targeting and Biodistribution Evaluated of Paramagnetic Solid Lipid Nanoparticles for Magnetic Resonance Imaging. *Nanomedicine* **2017**, *13*, 693−700.

(12) Nogueira, E.; Freitas, J.; Loureiro, A.; Nogueira, P.; Gomes, A. C.; Preto, A.; Carmoc, A. M.; Moreira, A.; Paulo, A. C. Neutral PEGlated Liposomal Formulation for Efficient Folate-Mediated Delivery of MCL1 siRNA to Activated Macrophages. *Colloids Surf., B* **2017**, *155*, 459−465.

(13) Angelopoulou, A.; Voulgari, E.; Diamanti, E. K.; Gournis, D.; Avgoustakis, K. Graphene Oxide Stabilized by PLA-PEG Copolymers for the Controlled Delivery of Paclitaxel. *Eur. J. Pharm. Biopharm.* **2015**, *93*, 18−26.

(14) Jung, H. S.; Lee, M. Y.; Kong, W. H.; Do, I. H.; Hahn, S. K. Nano Graphene Oxide-Hyaluronic Acid Conjugate for Target Specific Cancer Drug Delivery. *RSC Adv.* **2014**, *4*, 14197−14200.

(15) Coates, A.; Abraham, S.; Kaye, S. B.; Sowerbutts, T.; Frewin, C.; Fox, R. M.; Tattersall, M. H. On the Receiving End-Patient Perception of the Side-Effects of Cancer Chemotherapy. *Eur. J. Cancer Clin. Oncol.* **1982**, *19*, 203−208.

(16) Busam, K. J.; Capodieci, P.; Motzer, R.; Kiehn, T.; Phelan, D.; Halpern, A. C. Cutaneous Side-Effects in Cancer Patients Treated with

the Antiepidermal Growth Factor Receptor Antibody C225. *Br. J. Dermatol.* **2001**, *144*, 1169−1176.
(17) Prabhakar, N.; Näreoja, T.; Haartman, E.; Karaman, D. S.; Burikov, S. A.; Dolenko, T. A.; Deguchi, T.; Mamaeva, V.; Hänninen, P. E.; Vlasov, I. I.; Shenderova, O. A.; Rosenholm, J. M. Functionalization of Graphene Oxide Nanostructures Improves Photoluminescence and Facilitates Their Use as Optical Probes in Preclinical Imaging. *Nanoscale* **2015**, *7*, 10410−10420.
(18) Zhang, Z.; Wang, M.; Gao, D.; Luo, D.; Liu, Q.; Yang, J.; Li, Y. Targeted Raman Imaging Cells Using Graphene Oxide-Based Hybrids. *Langmuir* **2016**, *32*, 10253−10258.
(19) Thapa, R. K.; Choi, Y.; Jeong, J. H.; Youn, Y. S.; Choi, H. G.; Yong, C. S.; Kim, J. O. Folate-Mediated Targeted Delivery of Combination Chemoterapeutics Loaded Reduced Graphene Oxide for Synergistic Chemophotothermal Therapy of Cancer. *Pharm. Res.* **2016**, *33*, 2815−2827.
(20) Tian, J.; Luo, Y.; Huang, L.; Feng, Y.; Ju, H.; Yu, B. Y. Pegylated Folated and Peptide-Decorated Graphene Oxide Nanovehicle for In Vivo Targeted Delivery of Anticancer Drugs and Therapeutic Self-monitoring. *Biosens. Bioelectron.* **2016**, *80*, 519−524.
(21) Sudimack, J.; Lee, R. J. Targeted Drug Delivery Via the Folate Receptor. *Adv. Drug Delivery Rev.* **2000**, *41*, 147−162.
(22) Marino, F. Z.; Ronchi, A.; Accardo, M.; Franco, R. Detection of Folate Receptor-Positive Circulating tumor Cells by Ligand-Targeted Polymerase Chain Reaction in Non-Small Cell Lung Cancer Patients. *J. Thorac. Dis.* **2016**, *8*, 1437−1439.
(23) Phillips, T. The Role of Methylation in Gene Expression. *Nature Education* **2008**, *1* (1), 116.
(24) Parker, N.; Turk, M. J.; Westrick, E.; Lewis, J. D.; Low, P. S.; Learnon, C. P. Folate Receptor Expression in Carcinomas and Normal Tissues Determined by a Quantitative Radioligand Binding Assay. *Anal. Biochem.* **2005**, *338*, 284−293.
(25) Donnelly, J. G. Folic Acid. *Crit. Rev. Clin. Lab. Sci.* **2001**, *38*, 183−223.
(26) Abdel Nour, A. M.; Ringot, D.; Guéant, J. L.; Chango, A. Folate Receptor and Human Reduced Folate Carrier Expression in HepG2 Cell Line Exposed to Fumonisin B1 and Folate Deficiency. *Carcinogenesis* **2007**, *28* (11), 2291−2297.
(27) Matherly, L. H.; Hou, Z. Structure and Function of the Reduced Folate Carrier: A Paradigm of a Major Facilitator Superfamily Mammalian Nutrient Transporter. *Vitam. Horm.* **2008**, *79*, 145−184.
(28) Ai, J.; Xu, Y.; Li, D.; Liu, Z.; Wang, E. Folic Acid as Delivery Vehicles: Targeting Folate Conjugated Fluorescent Nanoparticles to Tumors Imaging. *Talanta* **2012**, *101*, 32−37.
(29) Low, P. S.; Kularatne, S. A. Folate-Targeted Therapeutic and Imaging Agents for Cancer. *Curr. Opin. Chem. Biol.* **2009**, *13*, 256−262.
(30) Sahu, S. K.; Mallick, S. K.; Santra, S.; Maiti, T. K.; Ghosh, S. K.; Pramanink, P. In Vitro Evaluation of Folic Acid Modified Carboxymethyl Chitosan Nanoparticles Loaded with Doxorubicin for Target Delivery. *J. Mater. Sci.: Mater. Med.* **2010**, *21*, 1587−1597.
(31) Mohapatra, S.; Mallick, S. K.; Maiti, T. K.; Ghosh, S. K.; Pramanink, P. Synthesis of Highly Stable Folic Acid Conjugated Magnetite Nanoparticles for Targeting Cancer Cells. *Nanotechnology* **2007**, *18*, 385102-1−385102-9.
(32) Frasconi, M.; Marotta, R.; Markey, L.; Flavin, K.; Spampinato, V.; Ceccone, G.; Echegoyen, L.; Scanlan, E. M.; Giordani, S. Multi-Functionalized Carbon Nano-Onions as Imaging Probes for Cancer Cells. *Chem. - Eur. J.* **2015**, *21*, 19071−19080.
(33) Dhar, S.; Liu, Z.; Thomale, J.; Dai, H.; Lippard, S. J. Targeted Single-Wall Carbon Nanotube-Mediated Pt(IV) Prodrug Delivery Using Folate as a Homing Device. *J. Am. Chem. Soc.* **2008**, *130*, 11467−11476.
(34) Chang, X.; Wang, Z.; Quan, S.; Xu, Y.; Jiang, Z.; Shao, L. Exploring the Synergetic Effects of Graphene Oxide (GO) and Polyvinylpyrrodione (PVP) on Poly(vinylylidenefluoride) (PVDF) Ultrafiltration Membrane Performance. *Appl. Surf. Sci.* **2014**, *316*, 537−548.
(35) Musico, Y. L. F.; Santos, C. M.; Dalida, M. L. P.; Rodrigues, D. F. Improved Removal of Lead (II) from Water Using a Polymer-Based Graphene Oxide Nanocomposite. *J. Mater. Chem. A* **2013**, *1*, 3789−3796.
(36) Peregrino, P. P.; Sales, M. J. A.; Silva, M. F. P.; Soler, M. A. G.; Silva, L. F. L.; Moreira, S. G. C.; Pateno, L. G. Thermal and Electrical Properties of Starch-Graphene Oxide Nanocomposites Improved by Photochemical Treatment. *Carbohydr. Polym.* **2014**, *106*, 305−311.
(37) Gao, W.; Alemany, L. B.; Ci, L.; Ajayan, P. M. New Insights into the Structure and Reduction of Graphite Oxide. *Nat. Chem.* **2009**, *1*, 403−408.
(38) Compton, O. C.; An, Z.; Putz, K. W.; Hong, B. J.; Hauser, B. G.; Brision, L. C.; Nguyen, S. Additive-Free Hydrogelation of Graphene Oxide by Ultrasonication. *Carbon* **2012**, *50*, 3399−3406.
(39) Park, S.; Hu, Y.; Hwang, J. O.; Lee, E. S.; Casabianca, L. B.; Cai, W.; Pott, J. R.; Ha, H. W.; Chen, S.; Oh, J.; Kim, S. O.; Kim, Y. H.; Ishii, Y.; Ruoff, R. S. Chemical Structures of Hydrazine-Treated Graphene Oxide and Generation of Aromactic Nitrogen Doping. *Nat. Commun.* **2012**, *3*, 1−8.
(40) Li, Y.; Chen, H.; Voo, L. Y.; Ji, J.; Zhang, G.; Zhang, G.; Zhang, F.; Fan, X. Synthesis of Partially Hydrogenated Graphene and Brominated Graphene. *J. Mater. Chem.* **2012**, *22*, 15021−15024.
(41) Cai, W.; Piner, R. D.; Stadermann, F. J.; Park, S.; Shaibat, M. A.; Ishii, Y.; Yang, D.; Velamakanni, A.; An, S. J.; Stoller, M.; An, J.; Chen, D.; Ruoff, R. S. Synthesis and Solid-State NMR Structural Characterization of ^{13}C-Labeled Graphite Oxide. *Science* **2008**, *321* (5897), 1815−1817.
(42) Kiem, R.; Knicker, H.; Körschens, M.; Kögel-Knabner, I. Refractory Organic Carbon in C-Depleted Arable Soils, as Studied by 13C NMR Spectroscopy and Carbohydrate Analysis. *Org. Geochem.* **2000**, *31*, 655−668.
(43) Hedges, J. I.; Baldock, J. A.; Gélinas, Y.; Lee, C.; Peterson, M. L.; Wakeham, S. G. The Biochemical and Elemental Compositions of Marine Plankton: A NMR Perspective. *Mar. Chem.* **2002**, *78*, 47−63.
(44) Schöning, I.; Morgenroth, G.; Kögel-Knabner, I. O/N-Alkyl and Alkyl are Stabilised in Fine Particle Size Fractions of Forest Soils. *Biogeochemistry* **2005**, *73*, 475−497.
(45) Bonechi, C.; Donati, A.; Lampariello, R.; Martini, S.; Picchi, M. P.; Ricci, M.; Rossi, C. Solution Structure of Folic Acid Molecular Mechanics and NMR Investigation. *Spectrochim. Acta, Part A* **2004**, *60*, 1411−1419.
(46) Nogueira, R. F.; Boffo, E. F.; Tavares, M. I. B.; Moreira, L. A.; Tavares, L. A.; Ferreira, A. G. The Use of Solid State NMR to Evaluate the Carbohydrates in Commercial Coffee Granules. *Food Nutr. Sci.* **2011**, *2*, 350−355.
(47) Murakami, M.; Ishida, H.; Kaji, H.; Horri, F. Solid-State 13CNMR Studies of the Structure and Chain Conformation of Thermotropic Liquid Crystalline Polyether Crystallized from the Liquid Crystalline Glassy Phase. *Polym. J.* **2004**, *36*, 403−412.
(48) Wu, G. L.; Sun, P. C.; Lin, H.; Ma, J. B. The Secondary Structures of Poly(L-Alanine) Blocks in Some Diblock Copolymers of Poly(L-Alanine) Monomethyl Ether in the Solid State Characterized by Nuclear Magnetic Resonance and Infrared Spectrometry. *J. Mol. Struct.* **2004**, *689*, 143−146.
(49) Preston, C. M.; Shipitalo, S. E.; Dudley, R. L.; Fyfe, C. A.; Mathur, S. P.; Levesque, M. Comparison of 13CPMAS NMR and Chemical Techniques for Measuring the Degree of Decomposition in Virgin and Cultivated Peat Profiles. *Can. J. Soil Sci.* **1987**, *67*, 187−198.
(50) Almendros, G.; Dorado, J.; Gonzalez-Vila, F. J.; Blanco, M. J.; Lankes, U. 13C NMR Assessment of Decomposition Patterns During Composting of Forest and Shrub Biomass. *Soil Biol. Biochem.* **2000**, *32*, 793−804.
(51) Farrán, M. A.; Claramunt, R. M.; López, C.; Pinilla, E.; Torres, M. R.; Elguero, J. Structural Characterization of Alloxazine and Substituted Isoalloxazines: NMR-Xray Crystallography. *ARKIVOC* **2007**, *2007* (iv), 20−38.
(52) Ando, I.; Kameda, T.; Asakawa, N.; Kuroki, S.; Hurosu, H. Structure of Peptides and Polypeptides in the Solid States as

DOI: 10.1021/acsanm.7b00324
ACS Appl. Nano Mater. 2018, 1, 922−932

Elucidated by NMR Chemical Shift. *J. Mol. Struct.* **1998**, *441*, 213−230.
(53) Nalluri, B. N.; Devineni, P. K.; Male, M. K.; Shaik, A. S.; Uppuluri, C. T. Studies on Development of Controlled Release Matrix Tablets of Camptothecin-an Anticancer Drug. *Indian J. Pharm. Educ.* **2015**, *49*, 292−300.
(54) Thakral, N. K.; Ray, A. R.; Bar-Shalom, D.; Eriksson, A. H.; Majumbar, D. K. Soluplus-Solubilized Citrated Camptothecin-A Potential Drug Delivery Strategy in Colon Cancer. *AAPS PharmSciTech* **2012**, *13*, 59−66.
(55) Li, Y.; Liu, R.; Yang, J.; Ma, G.; Zhang, Z.; Zhang, X. Dual Sensitive and Temporally Controlled Camptothecin Prodrug Liposomes Codelivery of siRNA for High Efficiency Tumor Therapy. *Biomaterials* **2014**, *35*, 9731−9745.
(56) Whitaker, R. D.; Ingebrigtsen, S. G.; Naderkhani, E.; Skar, M. L.; Flaten, G. E. Investigation of Parameters Influencing Incorporation, Retention and Cellular Cytotoxicity in Liposomal Formulations of Poorly Soluble Camptothecin. *J. Liposome Res.* **2013**, *23*, 298−310.
(57) Jang, D. J.; Moon, C.; Oh, E. Improved Tumor Targeting and Antitumor Activity Camptothecin Loaded Solid Lipid Nanoparticles by Preinjection of Blank Solid Nanoparticles. *Biomed. Pharmacother.* **2016**, *80*, 162−172.
(58) Martins, S. M.; Sarmento, B.; Nunes, C.; Lúcio, M.; Reis, S.; Ferreira, D. C. Brain Targeting effect of Camptothecin-Loaded Solid Lipid Nanoparticles in Rat after Intravenous Administration. *Eur. J. Pharm. Biopharm.* **2013**, *85*, 488−502.
(59) Wang, J.; Tian, Q.; Ding, F.; Yu, Y.; Wu, F. cRGDyK-modified camretastain A4-loaded graphene oxide nanosheets for targeted anticancer drug delivery. *RSC Adv.* **2015**, *5*, 40258−40268.
(60) Ma, M.; Xing, P.; Xu, S.; Li, S.; Chu, X.; Hao, A. Reversible pH-Responsive helical Nanoribbons Formed Using Camptothecin. *RSC Adv.* **2014**, *4*, 42372−42375.
(61) Cheng, J.; Khin, K. T.; Davis, M. E. Antitumor Activity of α-Cyclodextrin Polymer-Camptothecin Conjugates. *Mol. Pharmaceutics* **2004**, *1*, 183−193.
(62) Yang, X.; Wang, Z.; Niu, Y.; Chen, X.; Lee, S. M. Y.; Wang, R. Influence of Supramolecular Encapsulation of Camptothecin by Cucurbit[7]uril: Reduced Toxicity and Preserved Anti-Cancer Activity. *MedChemComm* **2016**, *7*, 1392−1397.
(63) Çirpanli, Y.; Bilensoy, E.; Dog, A. L.; Çalis, S. Comparative Evaluation of Polymeric and Amphiphilic Cyclodextrin Nanoparticles for Effective Camptothecin Delivery. *Eur. J. Pharm. Biopharm.* **2009**, *73* (1), 82−89.
(64) Kavitha, T.; Abdi, S. I. H.; Park, S. Y. pH-Sensitive Nanocargo Based on Smart Polymer Functionalized Graphene Oxide for Site-Specific Drug Delivery. *Phys. Chem. Chem. Phys.* **2013**, *15*, 5176−5185.
(65) Kavitha, T.; Kang, I. K.; Park, S. Y. Poly(N-vinyl Caprolactam) Grown on Nanographene Oxide as an Effective Nanocargo for Drug Delivery. *Colloids Surf., B* **2014**, *115*, 37−45.
(66) Russier, J.; Treossi, E.; Scarsi, A.; Perrozzi, F.; Dumortier, H.; Ottaviano, L.; Meneghetti, M.; Palermo, V.; Bianco, A. Evidencing the Mask Effect of Graphene Oxide: a Comparative Study on Primary Human and Murine Phagocytic Cells. *Nanoscale* **2013**, *5* (22), 11234−11247.
(67) Luna, L. A. V.; Moraes, A. C. M.; Consonni, S. R.; Pereira, C. D.; Cadore, S.; Giorgio, S.; Alves, O. L. Comparative *In vitro* Toxicity of a Graphene Oxide-Silver Nanocomposite and the Pristine Counterparts toward Macrophages. *J. Nanobiotechnol.* **2016**, *14* (1), 1−17.
(68) Liu, L. F.; Desai, S. D.; Li, T.-K.; Mao, Y.; Sun, M. E. I.; Sim, S.-P. Mechanism of Action of Camptothecin. *Ann. N. Y. Acad. Sci.* **2000**, *922* (1), 1−10.
(69) Elmore, S. Apoptosis: A Review of Programmed Cell Death. *Toxicol. Pathol.* **2007**, *35* (4), 495−516.
(70) Ranji-Burachaloo, H.; Karimi, F.; Xie, K.; Fu, Q.; Gurr, P. A.; Dunstan, D. E.; Qiao, G. G. MOF-Mediated Destruction of Cancer Using the Cell's Own Hydrogen Peroxide. *ACS Appl. Mater. Interfaces* **2017**, *9* (39), 33599−33608.

DOI: 10.1021/acsanm.7b00324
ACS Appl. Nano Mater. 2018, 1, 922−932